Journal of Science and Technology in Civil Engineering, HUCE, 2023, 17 (4): 80–94

NUMERICAL SIMULATION FOR THE FLEXURAL RESPONSE OF LARGE-SPAN UHPFRC PRESTRESSED COMPOSITE BOX GIRDER

Viet-Chinh Mai[a,*], Xuan Dai Nguyen[a], Canh Duc Nguyen[a]

[a]*Institute of Techniques for Special Engineering (ITSE), Le Quy Don Technical University, 236 Hoang Quoc Viet street, Bac Tu Liem district, Hanoi, Vietnam*

Article history:
Received 27/7/2023, Revised 02/11/2023, Accepted 06/11/2023

Abstract

Large-span girders serve as crucial components of contemporary infrastructure. For the design and analysis of these structures, a thorough comprehension of their structural behavior, particularly in terms of flexural response, is necessary. With its superior mechanical characteristics and greater durability, Ultra-High Performance Fiber Reinforced Concrete (UHPFRC) has significantly changed the construction business in recent years. Due to their potential for achieving longer spans, reduced construction time, and enhanced loading capacity, UHPFRC composite box girders have attracted a lot of attention. Comprehensive investigations are required to study the flexural behavior of large-span UHPFRC composite box girders under various loading conditions in order to ensure their safe and effective use. The study aims to provide an in-depth awareness of the loading capacity, deflection characteristics, and failure mechanisms exhibited by these girders by applying finite element analysis (FEA) techniques. The findings of the current investigation might inform the creation of large-span UHPFRC girder designs that are more effective and dependable, promoting sustainable and resilient infrastructure for the future.

Keywords: ultra-high performance fiber reinforced concrete (UHPFRC); large-span girder; composite box girder; smeared crack model; flexural response.

https://doi.org/10.31814/stce.huce2023-17(4)-07

1. Introduction

In the construction sector, large-span girders serve as important structural components since they allow for the establishment of large expanses without the need for intermediary supports [1, 2]. Reducing deflections, decreasing weight while preserving structural integrity, and guaranteeing adequate resistance to different loads, such as dead loads, live loads, and environmental conditions, are some of the unique challenges associated with large-span girders [3–5]. Ultra-High Performance Fiber Reinforced Concrete (UHPFRC) is considered as an advanced concrete. The UHPFRC mix design normally includes cement, filler (silica fume, silica floor, blast furnace slag), fine aggregates, water, superplasticizer and fibers. As compared to normal concrete, UHPFRC exhibits greater tensile and compressive strength as well as exceptional impact and crack resistance [6–10]. UHPFRC is a material that has drawn a lot of attention in the field of civil engineering because of its exceptional mechanical characteristics and durability [11, 12]. Pushing the boundaries regarding construction technology, UHPFRC offers new opportunities for creative designs, including longer spans, smaller cross-sections, and enhanced structural robustness.

A few researchers have carried out an experimental examination concerning the flexural behavior of UHPFRC box girders. Graybeal et al.'s study [13] for UHPFRC- prestressed I-girders, In-Hwan Yang et al.'s study for T-shape girders [14], and Qing-Young Guo et al.'s study [15] for segmental box shaped girders are a few examples. Other recent studies include those by Min-Seon Jeong et

*Corresponding author. *E-mail address:* maivietchinh@lqdtu.edu.vn (Mai, V.-C.)

al. [16] and Lee Seung-Jae et al. [17] for U-shaped segmental box girders as well as precast UHPFRC beams with prestressed bolted hybrid joints of Zhang et al. [18]. More research is required for large-span girders even if the aforementioned studies help us understand the flexural behavior of prestressed UHPFRC box girders. Though there exists a sizable amount of literature on numerical simulation regarding the flexural response of normal UHPFRC structures, yet lacks numerous studies of large-scale components in the simulation sector. Three various length, prestressed UHPFRC I-girders and four UHPFRC pi-girders were the subjects of research by Chen.L. et al. [19]. In contrast to pi-girders, which are 7.6 meters long, I-girders span are 24.4 meters and 9.2 meters, respectively. By using ABAQUS, the numerical simulation was carried out. In order to fully leverage the superior mechanical properties of UHPFRC over span lengths up to 41 m, Gang Zang et al. [20] concentrated on constructing a series of finite element-optimized sections of pi-girders. A calibrated and experimentally validated finite element model was utilized to conduct the study. Applying ABAQUS 6.11, the finite element models were analyzed. A group of UHPFRC pi-girders was created for spans up to 41.1 m as the study's conclusion. On a 30M UHPFRC box girder, Baochun Chen et al. [21] studied using both experimental and numerical methods. Initially, the structure of the box girder was altered to reduce the cost of UHPFRC applications. The box girder was akin to the primary UHPFRC Bridge from Shijiazhuang to Cixian in China before optimization. ABAQUS software was employed to perform the FE analysis, and the findings provided a good simulation of the behaviors of the UHPFRC structures.

More finite element analyses are required for large-scale UHPFRC structures, pursuant to the literature review. Studying the flexural response and performance of large-span UHPFRC box girders under loads is the primary objective of this study. Through the current work, engineers and researchers can acquire a useful knowledge regarding the performance and potential application of these novel structural elements.

2. Finite Element Analysis

In the present study, the flexural behavior of the 55m UHPFRC prestressed composite box girder is analyzed on the Midas FEM platform. Standard for design of UHPFRC structures in Vietnam is not available, the design of UHPFRC prestressed box girder follows the instructions in Korean standards. The UHPFRC box girder is assembled out of three segments that are U-shaped, as shown in Fig. 1. The cross-section A-A is formed at the support position as the full section, as depicted in Fig. 2(a). According to Fig. 2(b), the thickness of the U-girder's bottom flange ranges from 500 mm to 250 mm. As can be seen in Figs. 2(c) and 2(d), the thickness at the girder's midsection is applied with a constant value of 250 mm. The UHPFRC deck plate has the thickness of 50 mm while the upper slab reinforced by high strength concrete of 250 mm thickness. The U-girder's web contains no steel reinforcement bars while the T1 to T7 corresponds to the position of the pre-stressed tendons. To strengthen the stiffness of the HSC slab, steel bars with a diameter of 20 mm designated by S1, S2, and S3 are placed with a spacing of 125 and 250 mm, respectively.

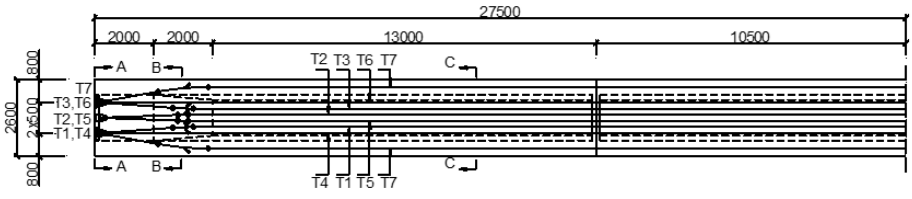

(a) Plan view

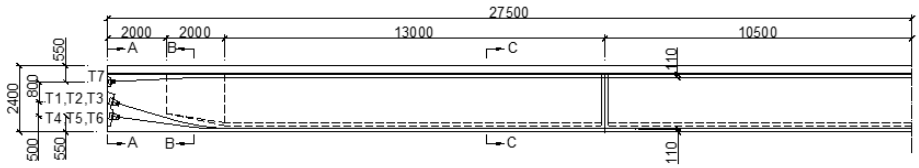

(b) Elevation view

Figure 1. Plan and elevation view of UHPFRC composite box girder

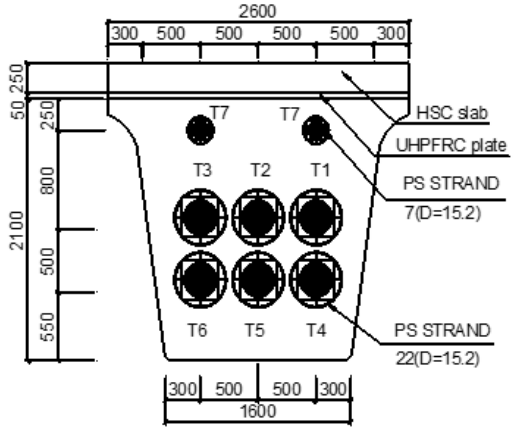

(a) Cross section A-A

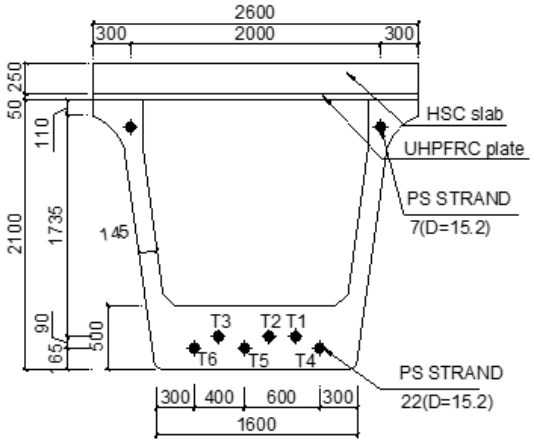

(b) Cross section B-B

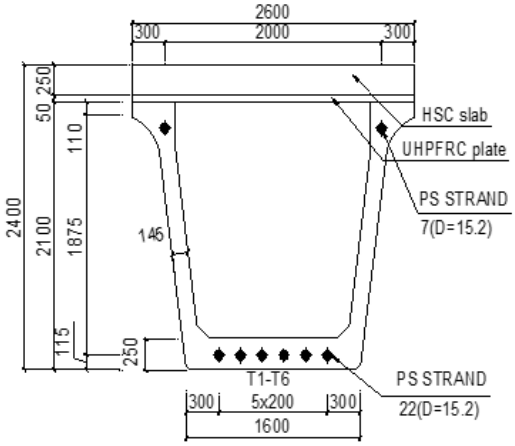

(c) Cross section C-C

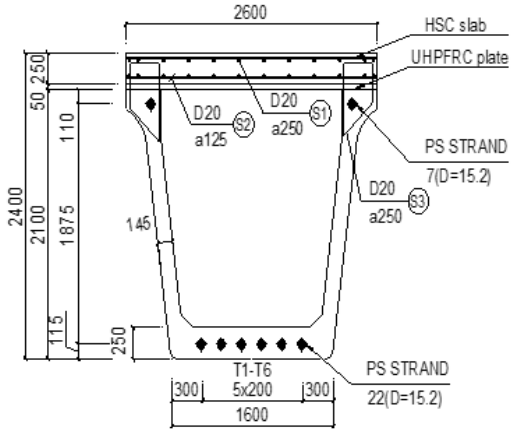

(d) Detail of steel reinforcement bars

Figure 2. Cross sections of UHPFRC composite box girder

2.1. Material Model

In order to simulate the behavior of brittle material like concrete, some famous models can be utilized, such as Drucker-Prager [22], Concrete Damaged Plasticity [23], Peri Dynamics (PD) model [24], discrete crack method [25] or smeared crack model [26]. The smeared crack model serves as a numerical method for simulating the behavior of materials with inherent crack formation and propagation in structural analysis. Instead of directly describing individual cracks, this approach assumes cracks as scattered discontinuities. It enables to the simulation of the beginning, propagation, and

interaction of cracks inside a material, giving details on the overall response of the structure. Researchers can analyze the structural integrity, forecast failure mechanisms, and determine the loading capability of diverse structures under varied loading circumstances by taking into account the behavior of smeared cracks [27]. The smeared crack model is adopted for the current study's simulation of UHPFRC behavior due to its advantages.

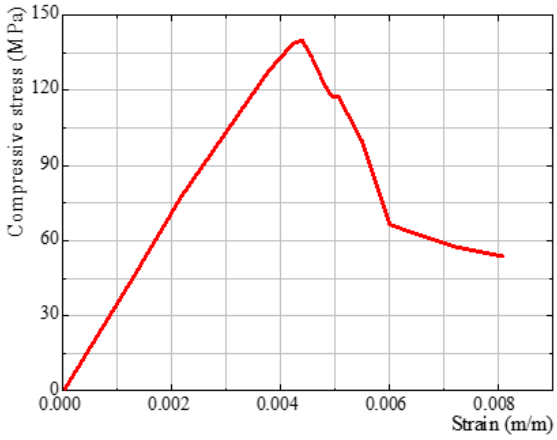

(a) Compressive stress-strain of UHPFRC

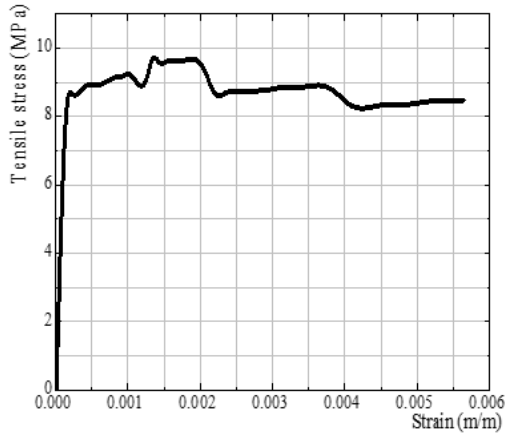

(b) Tensile stress-strain of UHPFRC

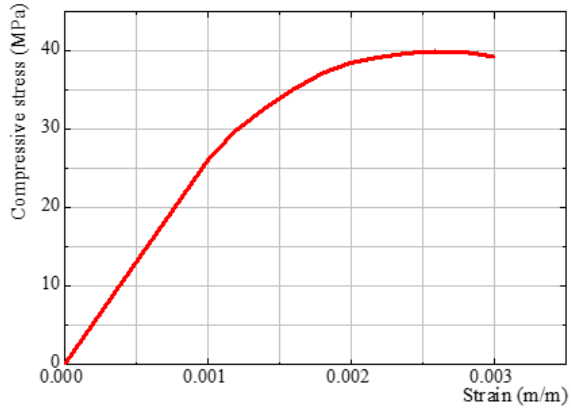

(c) Compressive stress-strain of HSC

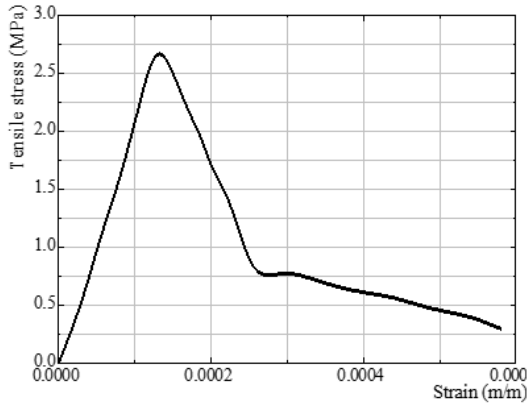

(d) Compressive stress-strain of HSC

Figure 3. Mechanical properties of concrete material

Figs. 3(a) and 3(b) presents the UHPFRC tensile and compressive behavior curves, which are derived using the approach suggested by Helou et al. [28]. The UHPFRC's highest compressive strength is 140 MPa at 0.0044 strain, while its maximum tensile strength reaches 9.6 MPa at 0.002 value of strain. The stress-strain curves of 40MPa compressive strength HSC in the simulation model are shown in Figs. 3(c) and 3(d).

Table 1. Material properties of prestressed tendons SWPC7A

Nominal diameter (mm)	Elastic modulus (MPa)	Poisson's ratio	Yielding load (kN)	Ultimate load (kN)
15.2	2e5	0.3	204	240

Table 2. Material properties of steel bar SD400

Elastic modulus (MPa)	Poisson's ratio	Weight density (Ton/m^3)	Yielding strength (MPa)	Ultimate strength (MPa)
$2e^5$	0.3	7.8	400	560

For prestressed composite box girders, tendon type SWPC7A, stipulated in the Korean standard [29], is deployed. Table 1 lists the tendons' structural characteristics. In more technical terms, the bottom flange includes 6×22 tendons and the top flange includes 2×7 tendons. The SWPC7A material has a 1470.8 MPa yielding strength and a 1730.3 MPa ultimate strength. Material characteristics of steel bar reinforcement SD400 are shown in Table 2.

2.2. *Simulation Model*

The unit 1D elements correspond to the model's horizontal reinforcement bars, vertical reinforcement bars, and prestressed tendons. Only axial forces are taken into account by these 1D elements, which is appropriate for their intended role. With the bar elements completely embedded in the concrete, the interaction between the 1D elements and the concrete elements is thought to be flawless. Fig. 4 shows the mesh model of composite box girder's cross-sections. Cross-sections composes of three parts: a UHPFRC U-section, a UHPFRC thin plate, and an HSC slab. The hexahedron element is effectively used in three-dimensional nonlinear analysis of concrete structure. Eight nodes constitute this element, and each one has three degrees of freedom. The hexahedron element involves crushing, cracking in three orthogonal directions, and plastic deformation. In nonlinear analysis, mesh size selection is critical. For the purpose to determine the most appropriate mesh size for the simulation model, investigations on mesh convergence were conducted by verifying three cases with minimum mesh sizes of 90 mm, 70 mm, and 50 mm, respectively. While a smaller mesh size produces findings that are more accurate, it also requires more processing to get those results. Under the four point-bending scheme, it appears that stress concentration is more likely occur in the girder's mid-span position. Therefore, the meshed section at this position with a minimum thickness of 50 mm and a minimum length of 60mm is proper. The coarser meshes with greater dimensions are employed for other locations.

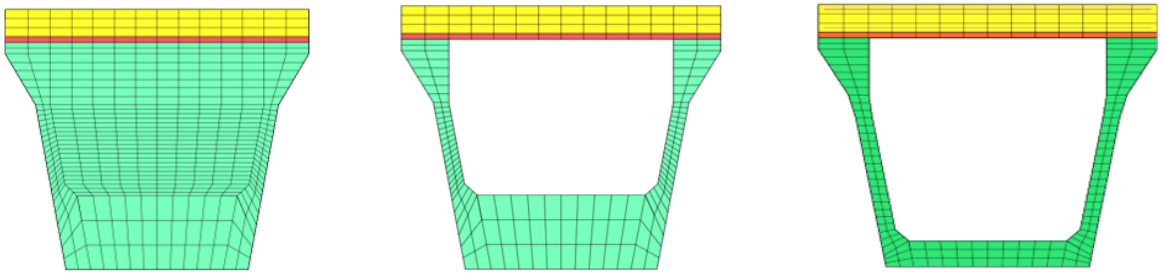

(a) In first segment (b) In second segment (c) In mid-span

Figure 4. Mesh model of UHPFRC composite box girder

The simulation model performs three different types of loads: self-weight, prestressed force, and deformation load. In Midas FEM, the self-weight is represented by the gravity load. Both ends of the tendon are receiving the prestressed force from jacking forces. Each tendon's prestressed force value is up to 150 kN. The loading capacity of a composite box girder is estimated using a four-point bending schematic diagram, in which two deflections are put on the top surface of an HSC slab 9 m

away from the girder's midspan. The simulation model's boundary condition is carried out as two simple rollers in supported positions, which is appropriate for a four-point bending scheme.

3. Results and discussion

3.1. Load-deflection curve

In order to shed light on the loading capacity of UHPFRC prestressed composite box girders, another numerical simulation was performed in which UHPFRC concrete was replaced by HSC material with a 40MPa compressive strength. Other details, such as the girder cross section, steel material parameters, and prestressed tendons, remain unchanged. The load-deflection curve at mid-span as well as simulation results of the UHPFRC composite box girder and HSC box girder are shown in Fig. 5 and Table 3.

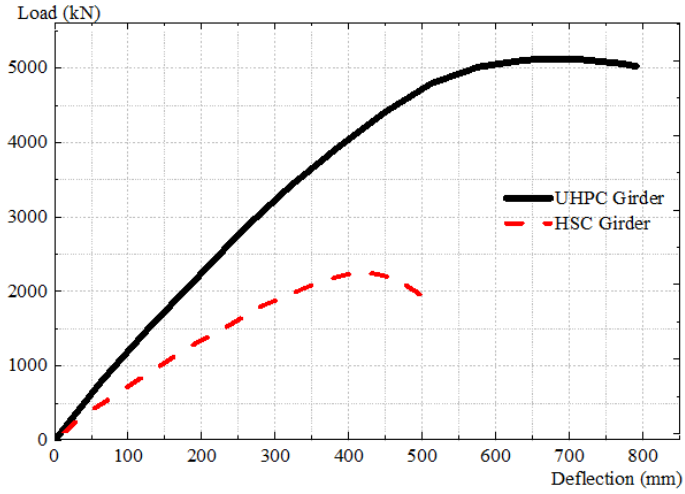

Figure 5. Load-deflection curve UHPFRC composite box girder and HSC box girder

Table 3. Loading capacity of UHPFRC composite girder and HSC girder

Case girder	Loading capacity (kN)	Deflection at peak load (mm)
UHPFRC composite girder	5126.22	704.23
HSC girder	2151.47	450.21
Disparity	238%	156%

For UHPFRC girder case, there are basically three stages to the curve. The first stage includes from the simulation beginning to the 1507.50 kN load. At this stage, the curve of load deflection behaves elastically without cracking. In the vicinity of a load of 1507.50 kN, or a deflection of 128.04 mm at the midspan, the first crack is observed. The second strain-hardening stage refers to the load range from 1507.50 kN to 5017.86 kN. The curve is introduced into the nonlinear stage. The number of cracks continues to grow quickly. The consequent deflection is anticipated to be 576.18 mm at a load of 5017.86 kN. The third stage from 5017.86 kN to 5126.22 kN. In this stage, also known as the plasticity behavior, the deflection proceeds to increase whereas the load nearly remains the same. More cracks propagate, and the existing ones is to be deeper. The curve begins to descend as the load is increased. The deflection that corresponds to the loading capacity of UHPFRC composite box girder's at 5126.22 kN is 704.23 mm.

The load-deflection curve of the HSC box girder essentially illustrates the various stages of behavior characteristic in a flexural member, as found in the UHPFRC girder model. Nonetheless, Fig. 5 reveals a difference in the third stage of ductile behaviour between the HSC and UHPFRC girders, with the UHPFRC girder showing a greater third-stage response. This difference may be explained to the significantly higher tensile and flexural strengths of UHPFRC relative to HSC material, resulting in a more marked plastic behaviour for the UHPFRC girder than the HSC girder. In addition, it ought to be note that the loading capacity of the UHPFRC girder is 2.38 times that of the HSC girder, as shown in Table 3. These results plainly demonstrate the superior performance of UHPFRC materials over conventional concrete as applied to flexural members.

3.2. Stress-Strain result

The composite box girder's strain data obtained from a four-point bending simulation that are derived at various points along the girder height, including in the middle span (M_i) and at the joint location (J_i), as shown in Fig. 6.

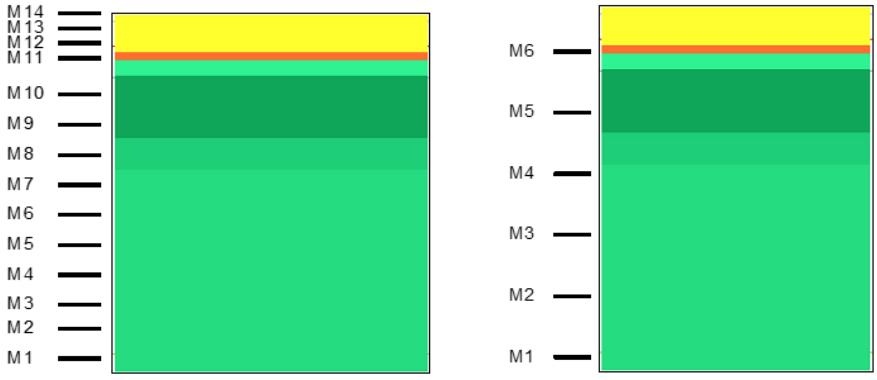

(a) At the mid-span (b) At joint position

Figure 6. Location of the strain gauge along the height of the UHPFRC box girder

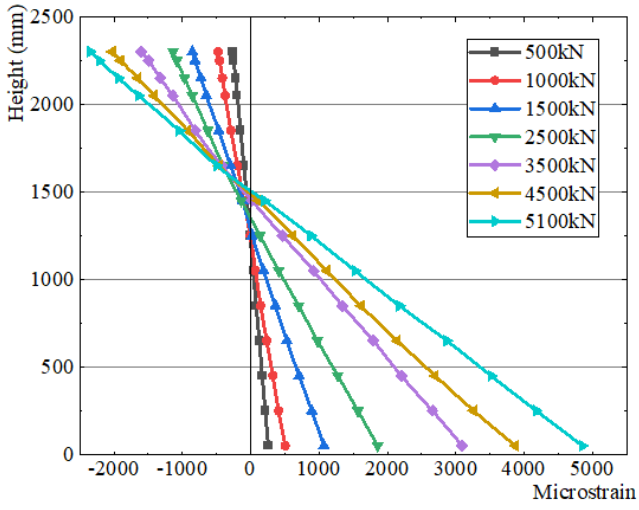

Figure 7. Strain profile of UHPFRC composite box girder at mid-span

The provided Figs. 7–8, which shows several loading phases, presents these strain results. The strains observable on the bottom surface (tension value) and top surface (compression value) of the

girder are relatively small during the first stage of the linear elastic curve. For example, when subjected to a 1000 kN load, the maximum tensile strain is 504.41$\mu\varepsilon$ and the minimum compressive strain is −478.72$\mu\varepsilon$. The strains on the upper and bottom surfaces of the girder dramatically rise as the load advances and enters the second stage. This stage reflects the girder's hardening behavior. The maximum positive strain and minimum negative strain under a load of 4500 kN are 3871.21$\mu\varepsilon$ and −2026.58$\mu\varepsilon$, respectively. The third stage features a relatively small load rise, yet the strains considerably increase. The maximum positive strain and minimum negative strain, for instance, are 4851.75$\mu\varepsilon$ and −2347.94$\mu\varepsilon$, respectively, for a load of 5100 kN. These values surpass those obtained at the 4500kN load level by 25% and 15%, respectively. This period's variation in strain is consistent with the plastic behavior shown in the load-deflection curve.

Although the strain values in tension and compression are noticeably lower than those in the mid-span of the composite box girder, the strain profile at the joint position (Fig. 8) exhibits a similar trend compared to the mid-span. Since the loads and deflections are significantly smaller than the girder's mid-span, this is entirely suitable.

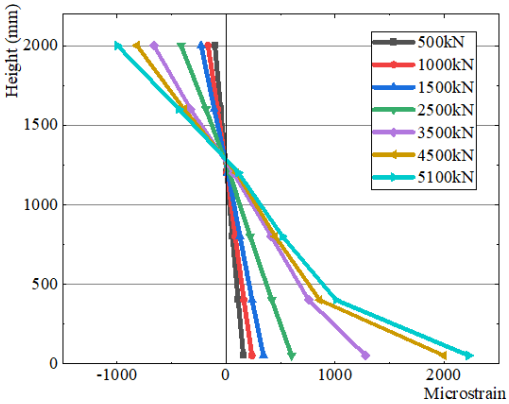

Figure 8. Strain profile of UHPFRC composite box girder at joint position

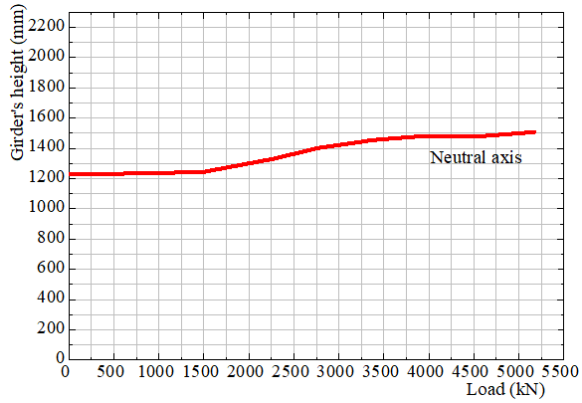

Figure 9. Neutral axis during the applied load at midspan

The position of the neutral axis at the mid-span of the girder is determined based on the predicted longitudinal strain profile obtained from the finite element analysis, as depicted in Fig. 9. The neutral axis exhibits the three stages of flexural behavior observed in the load-deflection curve of composite box girder. The neutral axis remains mostly steady during the initial phase, indicating sustainable values. This constant position signifies the linear elastic behavior of the composite box girder within the tension zone, where the height of the tension zone is not moved upward. The position of the neutral axis proceeds to rise considerably in the second stage. The composite box girder encounters a stage where many cracks start to form, and the girder exhibits a hardening behavior in the tensile region. As a result, the tensile zone's height rises. The gain in the location of the neutral axis is noticeably less in the third stage than that achieved in the second, demonstrating the plastic behavior of the composite box girder.

The curve of applied load versus tendon stress in the mid-span of the UHPFRC composite box girder are shown in Fig. 10(a). The stress in the upper tendons is 660.37 MPa for the maximum load under the four-point bending model of the girder, indicating that the upper tendons perform the elastic stage during simulation process. The stress on the bottom tendons is, however, noticeably higher than that on the upper tendons. The bottom tendons' maximum tensile stress, 1406.02 MPa, illustrates the plastic behavior. Comparing the load-stress curve to the relationship between applied load-strain, Fig. 10(b) shows the same trend. The upper tendons exhibit elastic behavior with a maximal positive

tensile strain of 3958.88$\mu\varepsilon$. The largest positive strain, measuring 12220.3$\mu\varepsilon$, is found in the bottom tendons, confirming plastic strain.

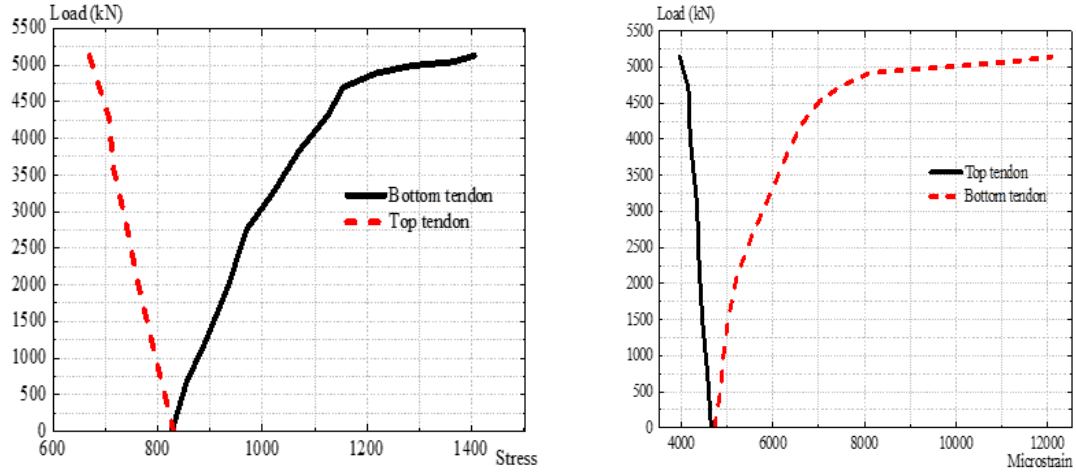

(a) Load-stress curve (b) Load-strain curve

Figure 10. Load-stress, strain curve of tendons at midspan

The HSC plate is reinforced with a double layer of longitudinal steel bars, referred to as S1 (upper layer) and S2 (lower layer), as depicted in Fig. 2(d). Fig. 11 represents the stress-strain relationship of the longitudinal steel bars under an applied load. The longitudinal steel bars reveal elastic behavior during the first and second stages, with maximum stresses below 250 MPa. The upper longitudinal steel bar, however, experiences plastic behavior in the third stage when the load reaches its peak value, with a maximum stress of close to 400 MPa. The top steel bar's measured peak strain is $-2369.23\mu\varepsilon$ (in compression). The stirrup steel bars (designated S3 in Fig. 2(d)) exhibit linear elastic behavior throughout the loading process, in contrast to the longitudinal steel bars, can be seen in Fig. 12. The bottom layer of the stirrup bars has a maximum stress and strain of 66 MPa and 349.07$\mu\varepsilon$, respectively.

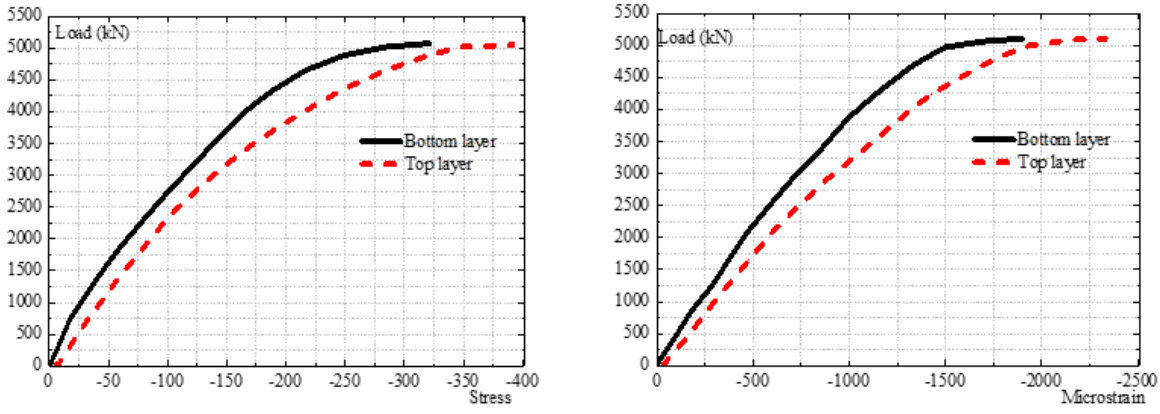

(a) Load-stress curve (b) Load-strain curve

Figure 11. Load-stress, strain curve of longitudinal steel bars at midspan

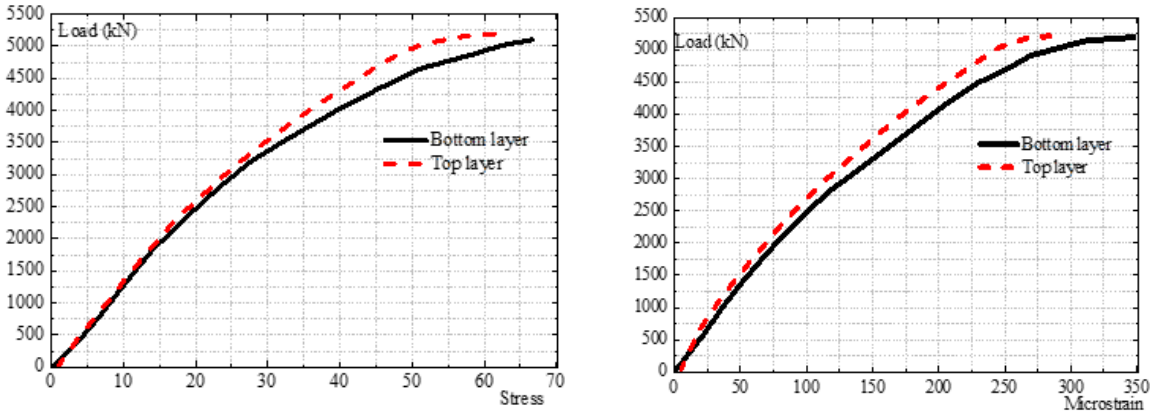

(a) Load-stress curve (b) Load-strain curve

Figure 12. Load-stress, strain curve of stirrup steel bars at midspan

Fig. 13 shows the stress-strain curve of HSC slab in compressive region. In the HSC slab, the compressive stress reach approximately 40 MPa, while the strain at positions 13 and 14 are $-2778.7\mu\varepsilon$ and $-2460.12\mu\varepsilon$, respectively. According to these results, the HSC slab exhibits strain-hardening behavior and crushing failures due to sufficient compressive strength.

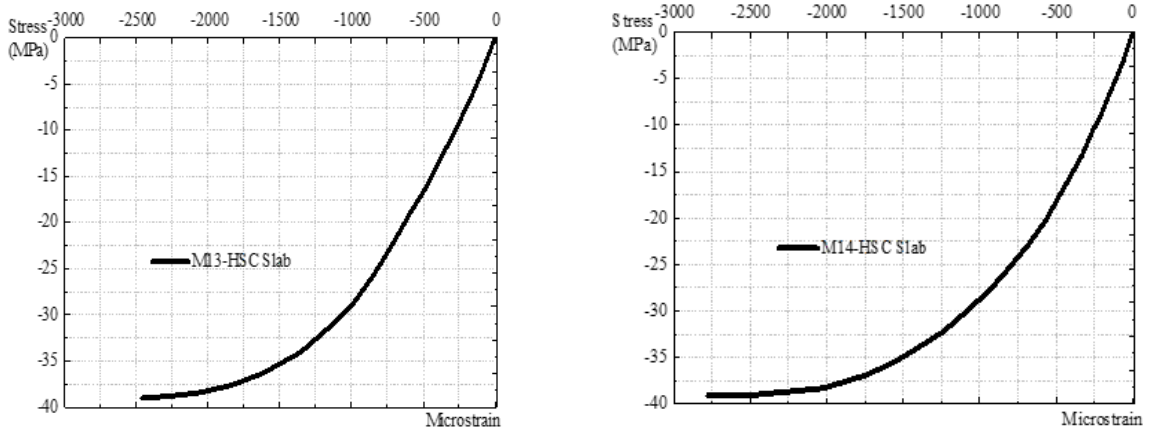

(a) At position M13 (b) At position M14

Figure 13. Stress-strain curve of HSC slab

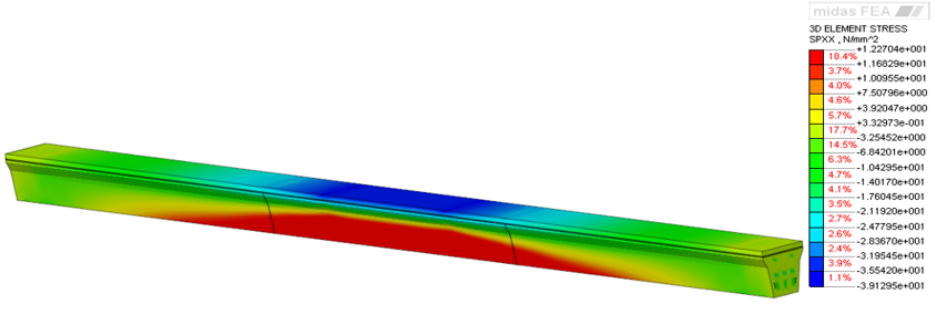

Figure 14. Stress contour of UHPFRC composite box girder under maximum loading

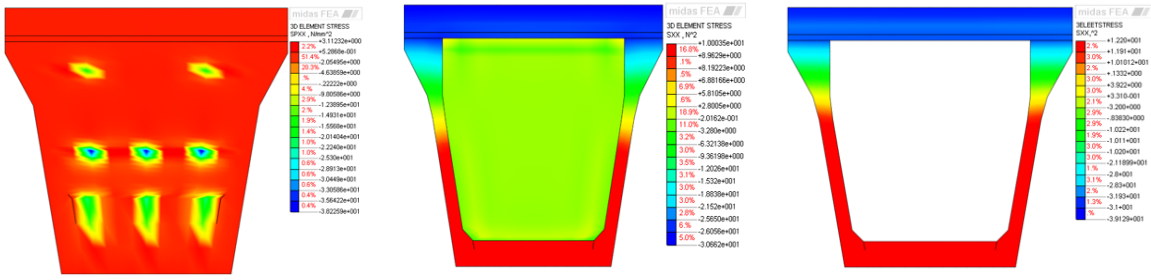

(a) Support position (b) Joint position (c) Mid-span position

Figure 15. Stress distribution at various cross sections in the UHPFRC box girder

The stress profile in the UHPFRC composite box girder is depicted in Fig. 14. It is clear that the red-colored tensile zone extends from the girder's midspan to the position near the support. In contrast, as the neutral axis shifts upwards (see Fig. 9 for more details), the compression zone narrows. The stress distribution is shown in Fig. 15 at various cross-sectional positions. The maximum tensile stress at the girder's support location, which is displayed in red, is just 3.1 MPa. On the other hand, the maximum compression stress, which has a value of −38.2 MPa (shown in blue), is found close to the region where the tendons and concrete interact. The bottom surface of the girder receives a maximum tensile stress of 10 MPa while the maximum compressive stress of the high-strength concrete slab in the joint position is −30.6 MPa. Additionally, relative to the support position, the tensile stress value rises enormously. Maximum tensile stress and maximum compressive stress are obtained at the mid-span location as 12.2 MPa and −39.1 MPa, respectively.

3.3. Cracking pattern

Initial crack occurs under a load of 1507.50 kN. Subsequently, its progression is observed as the applied load is gradually increased until the composite box girder fails. The estimation of crack width based on finite element analysis is performed for each strain gauge position and is summarized in Table 4.

Table 4. Crack propagation at midspan

Strain gauge	Position (mm)	Crack opening load (kN)	Initial width of crack (mm)	Crack width at maximum load (mm)
M1	50	1507.50	0.030	0.461
M2	250	2323.47	0.035	0.425
M3	450	2884.01	0.041	0.378
M4	650	3107.39	0.037	0.322
M5	850	3621.47	0.016	0.296
M6	1050	4124.89	0.018	0.251
M7	1250	4635.18	0.020	0.206

Fig. 16 shows the crack propagation under the external load and crack width (C_{wnn}). The UHPFRC girder exhibits no cracks during the initial stages of elastic behavior. Crack width in the second stage of inelastic behavior of the load-deflection curve range between 0.03 mm and 0.041 mm. These cracks are distributed along a length of 12.4 m in the middle of the span. The crack widths vary between 0.058 to 0.461 mm and stretch along a length of 27.8 m in the middle of the span at the maximum loading capacity of 5126.22 kN.

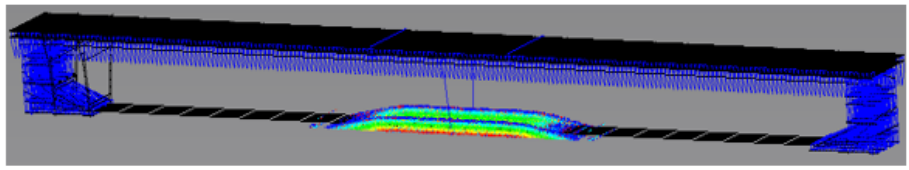

(a) In the second stage

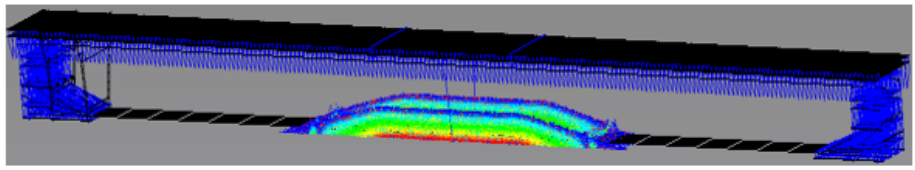

(b) In the third stage

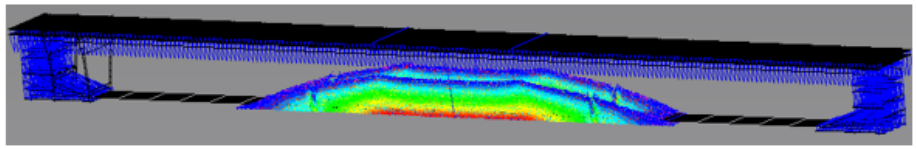

(c) At the maximum loading capacity

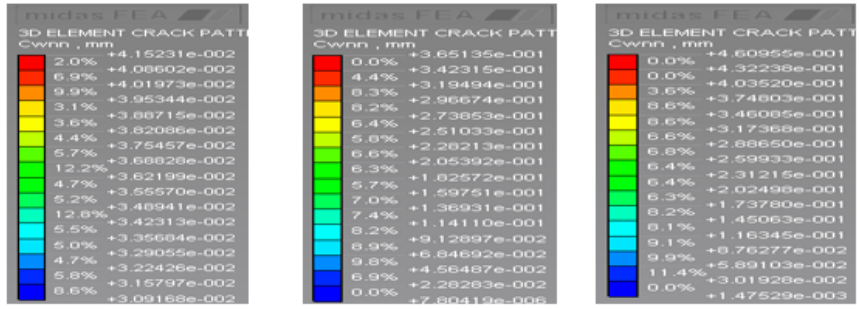

Crack width in the second stage

Crack width in the third stage

Crack width at the maximum loading capacity

Figure 16. Crack propagation during applied load and crack width

As shown in Fig. 17, the MIDAS FEA analysis identifies six different types of crack status in RC girder. Partially open loading cracks are represented by the blue hue, and partially open unloading cracks are indicated by the pink tint. Partially open loading cracks are recoverable and can close upon unloading, while partially open unloading cracks persist even after unloading. Two types of crack status emerge in the second stage: no crack yet and partially open loading, as depicted in Fig. 17(a). In the third stage, two crack statuses are observed, including no crack yet and partially open loading, as shown in Fig. 17(b). Crack status changed as a result of the increase in applied load, from partially open loading to partially open unloading behavior. At the maximum loading of 5126.22 kN, three types of crack status became apparent, as shown in Fig. 17(c): no crack yet, partially open loading, and partially open unloading.

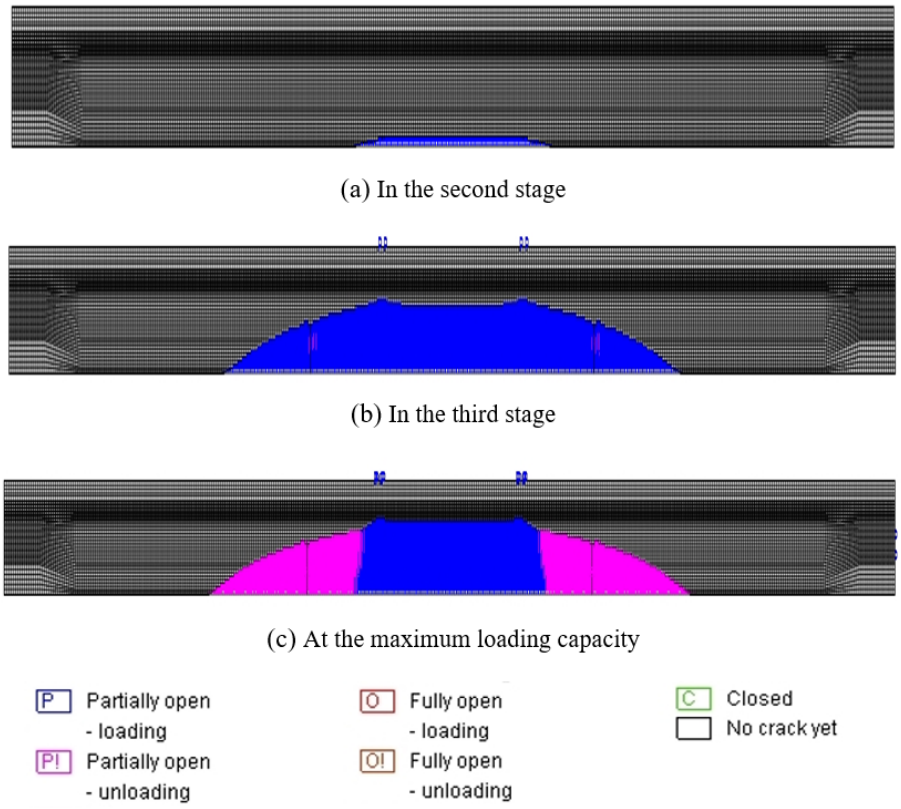

Figure 17. Crack status of girder

4. Conclusions

The aim of this study is to investigate the flexural behavior of the post-tensioned UHPFRC composite box girder. Using the smeared crack model in the Midas FEM software to simulate the nonlinear behavior of UHPFRC material and therefore determine the loading capacity, stress-strain relationship, and cracking pattern of the girder. Based on the results, the important conclusions can be drawn:

1. Flexural behavior of UHPFRC box girder exhibits characteristics resembling those of conventional flexural members. Nevertheless, the tensile zone of the girder is strengthened with UHPFRC material that possesses a high tensile strength result in enhancing appreciable bending stiffness and improved ductility in the overall response of the girder.

2. Even though there do not contain any stirrups or longitudinal reinforcing bars in the bottom flange or web, the UHPFRC composite box girder offers outstanding loading capacity due to the addition of prestressed tendons to resist flexural stresses generated by external loads.

3. Depending on precisely location, the prestressed tendons exhibit various characteristics. Under external load, the upper tendons experience compression and reflect a linear elastic stress at the maximum loading capacity of the girder. On the contrary, the bottom tendons reveal tensile stress in the cross section as subjected to external loads, as well as ductility behavior at the girder's peak load.

4. Once the HSC slab is crushed by compressive stress, the stress in the longitudinal reinforcing bars at the top surface of the girder concurrently approaches the yield stress level. It is necessary to improve the compressive strength of the HSC slab in order to fully exploit the possibilities of UHPFRC material and prestressed tendons.

Acknowledgement

This research is funded by Le Quy Don Technical University Research Fund under the grand number "23.1.74".

References

[1] Hemalatha, K., James, C., Natrayan, L., Swamynadh, V. (2021). Analysis of RCC T-beam and prestressed concrete box girder bridges super structure under different span conditions. *Materials Today: Proceedings*, 37:1507–1516.

[2] Ungureanu, V., Both, I., Burca, M., Radu, B., Neagu, C., Dubina, D. (2021). Experimental and numerical investigations on built-up cold-formed steel beams using resistance spot welding. *Thin-Walled Structures*, 161:107456.

[3] Rodriguez, S. (2004). Design of long span concrete box girder bridges: Challenges and solutions. In *Structures 2004: Building on the Past, Securing the Future*, 1–11.

[4] Antoniou, N., Nikolaidis, T., Baniotopoulos, C. C. (2014). Designing long-span steel girders by applying displacement control concepts. *Engineering Structures*, 59:21–27.

[5] Chen, Z.-S., Zhou, J.-T., Hu, G., Li, Y., Ma, H., Yao, G.-W. (2017). A novel movable scaffolding system (MSS) for a long-span curved girder bridge. *International Journal of Robotics and Automation*, 32(2).

[6] Hao, P. M., Thang, N. C., Thao, N. V., Tuan, N. V., Hai, L. N., Thuy, N. N., Man, N. X. (2022). Blast testing of ultra-high performance concrete fortifications using local materials. *Journal of Science and Technology in Civil Engineering (STCE)-HUCE*, 16(4):73–86.

[7] Liao, Q., Yu, J., Xie, X., Ye, J., Jiang, F. (2022). Experimental study of reinforced UHDC-UHPC panels under close-in blast loading. *Journal of Building Engineering*, 46:103498.

[8] Yang, J., Doh, J.-H., Yan, K., Zhang, X. (2022). Experimental investigation and prediction of shear capacity for UHPC beams. *Case Studies in Construction Materials*, 16:e01097.

[9] Tuan, N. V., Dong, P. S., Thanh, L. T., Thang, N. C., Hyeok, Y. K. (2021). Mix design of high-volume fly ash ultra high performance concrete. *Journal of Science and Technology in Civil Engineering (STCE) - HUCE*, 15(4):197–208.

[10] Ullah, R., Qiang, Y., Ahmad, J., Vatin, N. I., El-Shorbagy, M. A. (2022). Ultra-high-performance concrete (UHPC): a state-of-the-art review. *Materials*, 15(12):4131.

[11] Yu, Z., Wu, L., Yuan, Z., Zhang, C., Bangi, T. (2022). Mechanical properties, durability and application of ultra-high-performance concrete containing coarse aggregate (UHPC-CA): A review. *Construction and Building Materials*, 334:127360.

[12] Abdal, S., Mansour, W., Agwa, I., Nasr, M., Abadel, A., Onuralp Özkılıç, Y., Akeed, M. H. (2023). Application of ultra-high-performance concrete in bridge engineering: current status, limitations, challenges, and future prospects. *Buildings*, 13(1):185.

[13] Graybeal, B. A. (2006). *Structural behavior of ultra-high performance concrete prestressed I-girders*. Federal Highway Administration, Office of Infrastructure, United States.

[14] Yang, I.-H., Joh, C., Kim, B.-S. (2011). Flexural strength of large-scale ultra high performance concrete prestressed T-beams. *Canadian Journal of Civil Engineering*, 38(11):1185–1195.

[15] Guo, Q., Han, S.-M. (2014). Flexural behavior of ultra high performance fiber reinforced concrete segmental box girder. *Journal of the Korea Concrete Institute*, 26(2):109–116.

[16] Jeong, M.-S., Park, S.-Y., Han, S.-M. (2017). Ductile behavior of ultra high performance fiber reinforced concrete segmental box girder. *Journal of the Korean Recycled Construction Resources Institute*, 5(3): 282–289.

[17] Lee, S.-J., Makhbal, T.-O., Kim, S.-T., Han, S.-M. (2017). Flexural behavior of segmental U-girder and composite U-girder using ultra high performance concrete. *Journal of the Korean Recycled Construction Resources Institute*, 5(3):290–297.

[18] Zhang, Y., Zhu, P., Shi, J. (2020). Flexural behavior of precast UHPC beam with prestressed bolted hybrid joint. *Engineering Structures*, 206:110100.

[19] Chen, L., Graybeal, B. A. (2010). *Finite element analysis of ultra-high performance concrete: Modeling structural performance of an AASHTO type II girder and a 2nd generation pi-girder*. Federal Highway Administration, United States.

[20] Zhang, G., Graybeal, B. A. (2015). Development of UHPC Pi-Girder Sections for Span Length up to 41 m. *Journal of Bridge Engineering*, 20(3).

[21] Chen, B., Xilun, M., Zhou, J. (2018). Experimental Study on a Full Scale 30M Span UHPC Box. In *2nd International Conference on UHPC Materials and Structures (UHPC2018-China)*.

[22] Drucker, D. C., Prager, W. (1952). Soil mechanics and plastic analysis or limit design. *Quarterly of Applied Mathematics*, 10(2):157–165.

[23] Le Minh, H., Khatir, S., Abdel Wahab, M., Cuong-Le, T. (2021). A concrete damage plasticity model for predicting the effects of compressive high-strength concrete under static and dynamic loads. *Journal of Building Engineering*, 44:103239.

[24] Peng, R.-X., Qiu, W.-L., Jiang, M. (2021). Application of a micro-model for concrete to the simulation of crack propagation. *Theoretical and Applied Fracture Mechanics*, 116:103081.

[25] Willam, K., Carol, I. (1995). Discrete versus smeared crack analysis. In *Proceedings of the 2nd International Association of Fracture Mechanics for Concrete and Concrete Structures*, volume 3, Aedificatio Publ., 1885–1892.

[26] Petrangeli, M., Ožbolt, J. (1996). Smeared crack approaches—material modeling. *Journal of Engineering Mechanics*, 122(6):545–554.

[27] Mukhtar, F., El-Tohfa, A. (2023). A review on fracture propagation in concrete: Models, methods, and benchmark tests. *Engineering Fracture Mechanics*, 281:109100.

[28] El-Helou, R. G., Graybeal, B. A. (2019). The Ultra Girder: A Design Concept for a 300-foot Single Span Prestressed Ultra-High Performance Concrete Bridge Girder. In *Second International Interactive Symposium on UHPC*, Iowa State University Digital Press.

[29] K.C.I. (2016). *Concrete structure design standard*. Korea Concrete Institute.